An investigation of the tensile deformation and failure of an epoxy/Cu interface using coarse-grained molecular dynamics simulations

2014 Modelling Simul. Mater. Sci. Eng. 22 065011

(http://iopscience.iop.org/0965-0393/22/6/065011)

IOP Publishing Modelling and Simulation in Materials Science and Engineering

Modelling Simul. Mater. Sci. Eng. **22** (2014) 065011 (21pp) doi:10.1088/0965-0393/22/6/065011

An investigation of the tensile deformation and failure of an epoxy/Cu interface using coarse-grained molecular dynamics simulations

Shaorui Yang[1] **and Jianmin Qu**[1,2]

[1] Department Mechanical Engineering, Northwestern University, Evanston, IL, 60208, USA
[2] Department of Civil and Environmental Engineering, Northwestern University, Evanston, IL, 60208, USA

E-mail: j-qu@northwestern.edu

Received 30 March 2014, revised 24 June 2014
Accepted for publication 3 July 2014
Published 6 August 2014

Abstract

In this study, a coarse-grained model is developed to describe the interatomic interactions between a cross-linked epoxy and a copper substrate. Based on this model, the tensile deformation and failure of an epoxy/Cu bimaterial is studied. Attention is given to the microstructural evolution near the epoxy/Cu interface, and its effects on the overall stress–strain behavior of the bimaterial. It is found that, under uniaxial strain, plastic deformation in the epoxy/Cu bimaterial is localized to a thin layer of epoxy next to the epoxy/Cu interface. This discovery enables the definition of an interfacial zone. Consequently, a cohesive zone model at the continuum level could potentially be constructed where the separation of the interface is given by the stretching of the interfacial zone computed from the coarse grain simulations.

Keywords: epoxy molding compound, interface, coarse-grain, molecular dynamics simulation

(Some figures may appear in colour only in the online journal)

1. Introduction

Polymer/metal interfaces are ubiquitous in engineering applications. In microelectronics, in particular, epoxy/Cu interfaces are prevalent. However, experimental measurements of interfacial strength or fracture toughness [1–3] are extremely time-consuming and expensive.

The ability to predict the interfacial strength of such interfaces has been a long-desired goal. Recent advances in atomistic level simulations and computing power have enabled significant progress toward such predictive capabilities. For example, molecular statics (e.g., energy minimization), molecular dynamics (MD) and Monte Carlo simulations have been used in recent years to study the mechanical behavior of polymer/metal interfaces [4–6]. In addition to simulating the deformation and failure, these simulation techniques also capture: (1) the deformation-driven microstructural evolution near the interface and (2) how such evolution affects the overall mechanical behavior of the polymer/metal bimaterial.

In our previous works [6, 7], we reported full atomic MD studies of tensile strength and deformation/failure mechanisms in an epoxy/Cu bimaterial. Based on the polymer consistent force field (PCFF) [8, 9], our MD simulations investigated the effects of strain rate, temperature, cross-link density and epoxy monomer functionality. Such full atomic MD simulations provide useful insights regarding the atomistic interactions near the epoxy/Cu interface. However, we also found that the material volume that can be simulated by the full atomic MD is rather small. The behavior of such a small material volume may not be representative of the macroscopic behavior of the epoxy/Cu interface. More importantly, the PCFF used in the full atomic MD is not capable of describing the failure of atomic bonds in the epoxy, which severely limits its ability to simulate material failure.

In order to simulate the behavior of a larger material volume, coarse-graining approaches have been developed. In such coarse-grained (CG) models, atoms are lumped into groups. Each group is called a bead. Once the interaction among the beads is described by a potential function, the beads can be treated as 'super atoms' and MD simulations can be conducted for the ensemble of the beads. One advantage of such course-grained molecular dynamics (CGMD) simulations is the reduced the number of degrees of freedom, which enables the simulation of a larger material volume. The other advantage is the larger mass of the beads, which increases the integration time step in simulating a physical process.

The CGMD simulations have been extensively applied to polymeric materials to predict material properties and to study physical processes. Methodologies of coarse-graining and multi-scale modeling in polymer science have been comprehensively reviewed in several review articles [10–12]. There are several approaches to developing and parametrizing the inter-bead potentials suitable for CGMD simulations. One of these methods is the Boltzmann inversion [13–16] or inverse Monte Carlo technique [17] which starts from potential mean force and iteratively adjusts parameters to match distribution functions. Another approach is the force matching method which aims to minimize the difference between the CG and full atomic data on inter-bead forces [18]. A third approach is to use prescribed potential formulations and determine the parameters by fitting material properties of interests to experimental or full atomic data [19–21]. This approach was used in our earlier works [22, 23] to develop a CG model for the same cross-linked epoxy considered in this study. This CG model is able to predict material properties and property–structure correlations as predicted by full atomic MD simulations.

Most of the exiting CGMD simulations are for bulk materials. For polymer/metal interfaces, there is the additional challenge of coarse-graining the interfacial interactions between the polymer atoms and the metal substrate. There has been little work done in this regard. Site *et al* [24] studied the adsorption of bisphenol-A-polycarbonate (BPA-PC) on the surface of nickel (Ni) (1 1 1) using CGMD simulations. The BPA-PC versus Ni interaction in their CG model is described by a planar Lennard-Jones 10–4 potential, in which the parameters are obtained from quantum mechanical calculations. This CG model was later further developed to account for chain-end orientations on the adsorption [25]. In another work, Farah *et al* [26] used a planar Lennard-Jones potential, with a 9–3 functional form to calculate

the interactions between CG beads and the planar surface. However, this work is a parametric study on the effect of tuning the potential well depth. The potential was not parametrized rigorously. Wong *et al* [5] studied the interaction energy and equilibrium distance between an epoxy molding compound and the copper substrate. The work most relevant to the current investigation is that of Iwamoto [27–29], in which the author established a meso-scale model for an epoxy/Cu_2O interface. The Cu_2O substrate is CG in such a way that a 2×2 super cell is used as a bead.

The objective of this study is to understand the deformation behavior and failure mechanisms of epoxy/Cu interface by using CGMD simulations. Because of the lack of mature coarse-grained models for epoxy/Cu interfaces in the literature, first we need to develop an appropriate coarse-grained potential to describe the interaction between the epoxy and Cu atoms at their interface. This is discussed in section 2. In section 3, the procedure for carrying out the CGMD simulations of uniaxial strain deformation is discussed. Section 4 presents the simulation results and discussions. Specifically, section 4.1 presents the microstructure features near the epoxy/Cu interface. Section 4.2 presents the uniaxial stress–strain curves, and discovery of the interfacial zone over which much of the plastic deformation occurs, which enables the construction of the traction versus separation law for the cohesive zone model used in continuum mechanics. The effects of strain rate, temperature and conversion rate are discussed in sections 4.3 and 4.4, respectively. Finally, some concluding remarks are presented in section 5.

2. CG model development

2.1. CG force-field for bulk epoxy

The epoxy molding compound of our interest is an EPN–BPA system, composed of epoxy phenol novolac (EPN) as the epoxy monomer and bisphenol-A (BPA) as the cross-linking agent. Molecular structures of the monomers and the curing reaction mechanisms were discussed in [6, 7]. A CG model of this EPN–BPA system was developed in [22], which will be used in this study. For completeness, the model is briefly outlined below.

The constitutive monomers (3mer and 4mer of EPN and BPA) are represented as short chains of connected beads with identical mass M, Lennard-Jones potential-well depth ε and diameter σ. Beads interact with each other through the Lennard-Jones 12–6 potential, a harmonic angle bending potential and a quartic bond stretching potential that allows smooth bond breakage. These potentials are listed below,

$$U_{\mathrm{LJ}}(r) = 4\varepsilon\left[\left(\frac{\sigma}{r}\right)^{12} - \left(\frac{\sigma}{r}\right)^{6}\right], \tag{1}$$

$$U_b(r) = U_0 + k_4(r - r_c)^2(r - b_1 - r_c)(r - b_2 - r_c)H(r_c - r) + 4\varepsilon\left[\left(\frac{\sigma}{r}\right)^{12} - \left(\frac{\sigma}{r}\right)^{6} + \frac{1}{4}\right]H(2^{1/6}\sigma - r)H(r_c - r), \tag{2}$$

$$U_a^{(i)}(\theta) = k_\theta^{(i)}(\theta - \theta_0^{(i)})^2, \quad i = 1, 2, 3. \tag{3}$$

The optimized parameters in the above potentials were obtained in [22] and are listed in table 1.

2.2. CG model for metal substrate

To develop a CG model for the epoxy/Cu interface, the first task is to group Cu atoms into beads. The concept here is to use a virtual face-centered cubic crystalline structure, with an appropriate lattice constant to represent the CG Cu substrate. The lattice constant should not be

Table 1. Optimized parameters in the CG potentials.

M (g mol^{-1})	ε (kcal mol^{-1})	σ (Å)	k_4 (kcal mol^{-1} Å^{-4})	r_c (Å)	b_1 (Å)	b_2 (Å)
55.565	1.519	4.383	5.901	5.887	−3.326	0.0
U_0 (kcal mol^{-1})	$k_\theta^{(1)}$ (kcal mol^{-1} rad^{-2})	$k_\theta^{(2)}$	$k_\theta^{(3)}$	$\theta_0^{(1)}$(°)	$\theta_0^{(2)}$	$\theta_0^{(3)}$
102.082	2.395	2.899	0.613	100	180	180

too small, otherwise the advantage of reducing the number of particles through coarse-graining is lost; the lattice constant also should not be too large to prevent polymers from penetrating into the substrate, which is unphysical based on observations obtained from a previous full atomic study [30]. In the investigation by Stevens [31], the nearest-neighbor distance between the FCC substrate beads is chosen to be 1.204σ, where σ is the Lennard-Jones diameter of the epoxy beads. This choice is adopted here, which corresponds to a lattice constant of $1.204\sqrt{2}\sigma = 7.463$ Å.

In addition, to describe the interactions between the Cu beads, we link each Cu bead to its nearest neighbors on the face-centered cubic lattice site using a spring with a spring constant of $1000\varepsilon/\sigma^2 = 79.04\,\text{kcal}^{-1}\,\text{mol}\,\text{Å}^{-2}$). This is done to maintain the crystalline structure of the substrate during the MD simulations.

2.3. Metadynamics

Next, we construct our CG bimaterial potential based on the free energy surface of the epoxy/Cu system from an attached state to a detached state. This free energy surface will be computationally obtained by using a metadynamics method [32, 33]. The fundamental concept of the metadynamics method is to fill the system free energy well with a series of Gaussian potentials and to track the filled Gaussian to reconstruct the free energy landscape [4]. The definition of the Gaussian potential depends on the selection of a set of collective variables that are suitable for describing the physical process of interest. Let s_i, $i = 1, 2, \ldots, d$ be d number of collective variables. Then the Gaussian potential applied on the system at time t can be written as,

$$V(s,t) = \omega \sum_{\substack{t' = \tau_G, 2\tau_G, \cdots \\ t' < t}} \exp\left(-\sum_{i=1}^{d} \frac{[s_i(\boldsymbol{r}) - s_i(\boldsymbol{r}(t'))]^2}{2\delta_i^2}\right), \tag{4}$$

where s is a measure of the distance between the epoxy and the Cu substrate, δ_i is the Gaussian width of the ith collective variable and ω and τ_G are the Gaussian height and the frequency at which the Gaussian potential is added, respectively. Once the Gaussian potential is added to the system, forces due to this potential will be exerted onto micro-coordinates such as atom or bead positions. For example, let r_j be the system's jth degree of freedom ($j \leqslant 3N$; N is the number of atoms or beads), then the force on this degree of freedom is

$$-\frac{\partial V(s,t)}{\partial r_j} = -\sum_{i=1}^{d} \frac{\partial V(s,t)}{\partial s_i} \frac{\partial s_i(\boldsymbol{r})}{\partial r_j}. \tag{5}$$

This method was applied in [4] to study the intrinsic strength between epoxy and silica.

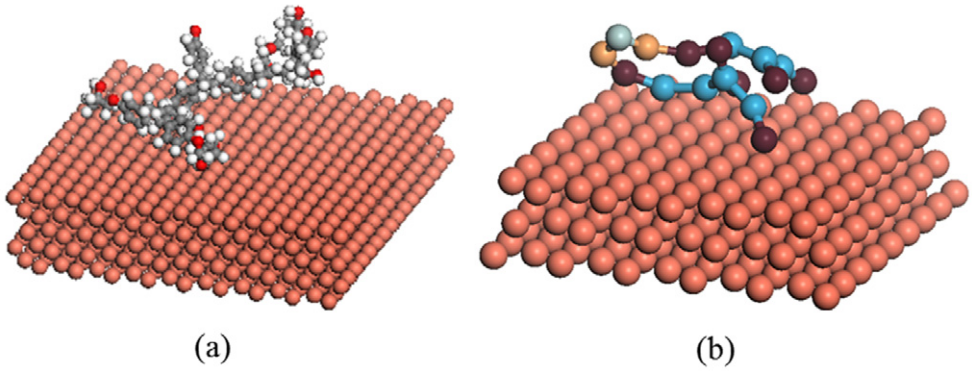

Figure 1. (*a*) Full atomic and (*b*) CG models of the representative molecule attached to the Cu substrate.

2.4. CG force-field for epoxy/Cu interaction

In the current investigation, a 3mer-EPN, a 4mer-EPN and a BPA monomer are linked to form a 'representative' molecule of the cross-linked epoxy. The representative molecule is attached to the Cu substrate as shown in figure 1(*a*). The Cu substrate has a surface area of 39.4×38.7 Å^2 and is periodic along both of the in-plane directions. It contains six layers (1 1 1) of atomic planes. The PCFF is used to describe the full atomic epoxy system. Between the epoxy molecules and the Cu substrate, the Lennard-Jones (9–6) potential and the sixth-power mixing rule are applied to calculate the van der Waals forces [6]. After the model geometry and force-field parameters are defined, the model is equilibrated using the NVT MD simulation at 300 K using the LAMMPS code [34].

To implement the metadynamics in MD simulations, the collective variable is chosen to be the distance s between the center of mass of the representative molecule and the surface of the Cu substrate. During our MD simulations, a Gaussian potential is added to the system periodically. Each time a Gaussian potential is added to the system, it adds forces to the system. Consequently, the distance s varies with increasing number of Gaussian potentials, but not necessarily monotonically. In other words, there is not a one-to-one correspondence between s and the number of Gaussian potentials. In fact, each value of s may be associated with many potentials depending on the total number of potentials added to the system. At a given time (i.e., after a certain number of Gaussian potentials are added to the system), metadynamics calculations can then identify which potentials are associated with a given distance s. Summation of these potentials gives the free energy associated with s at that particular time. One may then plot the free energy versus s curve for any given time. As time increases (i.e., as more potentials are added to the system), the free energy versus s curves eventually converge to a single one, which is called the free energy surface of the epoxy/Cu system. In this work, the software package PLUMED [35] is used to conduct the metadynamics calculations. During the NVT MD simulations at 300 K, a Gaussian potential of height $\omega = 0.005$ and width $\delta = 0.35$ is added at every 100 time steps. These choices of parameters were also used in [4] and found to be a good balance between accuracy and computational efficiency. Figure 2 shows the results of the metadynamics calculations. The convergence of the free energy surface is achieved at around 64 ns. With further calculation, the free energy surface will be the same. From the converged free energy surface (the blue curve in figure 2) the energy barrier between the attached and detached states is found to

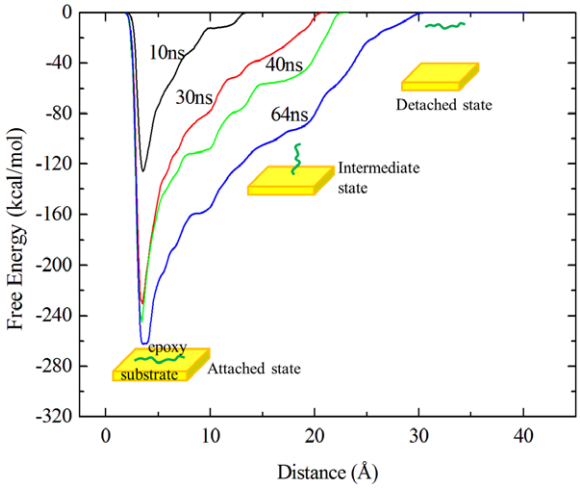

Figure 2. Free energy surface for the full atomic model obtained from the metadynamics calculations. Distance is from the center-of-mass of the epoxy molecule to the Cu substrate.

be approximately 262 kcal mol^{-1} and the equilibrium distance between the epoxy molecule's center of mass and the copper substrate surface is ∼3.68 Å.

In order to derive the CG model for the epoxy/Cu bimaterial, the Lennard-Jones 12–6 potential is used to describe the interactions between epoxy beads and the substrate beads. Let ε_{ew} and σ_{ew} be the two parameters of the Lennard-Jones potential function so that,

$$U_{ew} = 4\varepsilon_{ew}\left[\left(\frac{\sigma_{ew}}{r}\right)^{12} - \left(\frac{\sigma_{ew}}{r}\right)^{6}\right]. \tag{6}$$

The task is then to determine the two parameters, ε_{ew} and σ_{ew}. To this end, we first construct the CG model for the full atomic model of the epoxy molecule and Cu substrate system shown in figure 1(a). The corresponding CG model is shown in figure 1(b). Next, we compute the free energy surface of the CG epoxy molecule and Cu substrate system by using the same steps used to compute the free energy surface of the full atomic epoxy and Cu substrate system; see figure 2. The free energy surface so computed will depend on the values of ε_{ew} and σ_{ew} used. We postulate that if the free energy surface of the CG model matches that of the full atomic model, the corresponding values of ε_{ew} and σ_{ew} will be the optimal values for the potential given in (6).

Figure 3 plots the free energy surfaces using the CG bimaterial model with different Lennard-Jones potential parameters. A clear trend is the increase of the energy barrier from the attached to the detached states with respect to the potential depth ε_{ew}. The equilibrium distance between the mass center of the epoxy molecule and the substrate surface remains almost unchanged with changing ε_{ew}. Trial-and-error calculations show that the free energy surface becomes very close to that obtained from the full atomic model when $\sigma_{ew} = \sigma$ and $\varepsilon_{ew} = 3\varepsilon$, where σ and ε are the Lennard-Jones parameters for the CG epoxy; see (1) and table 1. Thus, this set of parameters will be used for the CGMD simulations of the epoxy/Cu bimaterial at the CG level.

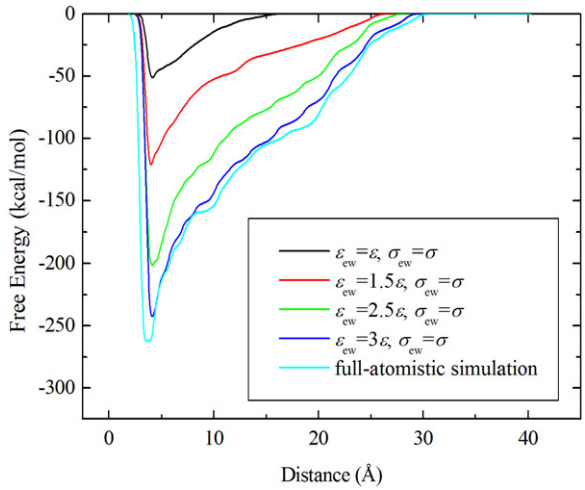

Figure 3. Free energy surfaces of the CG model computed using different CG Lennard-Jones parameters, compared to the free energy surface of the corresponding full atomic model. Distance is from the center-of-mass of the epoxy molecule to the Cu substrate.

3. CG study of tensile deformation of bimaterial

3.1. Equilibration

Having the CG models for the bulk epoxy and the epoxy/Cu interface, we are ready to study the mechanical property and behavior of epoxy/Cu bimaterial at a length scale that is typically inaccessible by full atomic simulations. The CG epxoy/Cu bimaterial model consists of a rectangular block for the epoxy siting on a Cu substrate containing four (1 1 1) atomic planes. Periodic boundary conditions are used on all the lateral surfaces. To build the simulation cell, beads representing epoxy and hardener monomers are randomly seeded inside the rectangular block. The stoichiometry ratio of 2 : 3 : 9 is used for the numbers of 3mer-EPN, 4mer-EPN and BPA. The model has a total of 7964 588 beads, corresponding to a physical volume of $\sim 89 \times 89 \times 79\,\mathrm{nm}^3$ (at 300 K).

3.2. Cross-linking

After the beads are randomly seeded, the system is cross-linked at 500 K using a time step of 5 fs, during which the top surface of the epoxy block and the bottom surface of the Cu substrate are kept traction free. As was described in [22], each epoxy monomer (EPN), depending on functionality, has either three or four reactive beads, and each hardener monomer (BPA) has two reactive beads. The chain length of the EPN monomer is either five or six, depending on the functionality, and the chain length of the BPA monomer is three. In the dynamic cross-linking process, we specify that if an EPN reactive bead is within a 5.7 Å radius of a BPA reactive bead, there is a chance of 1% that this EPN bead will form a bond with the BPA. For every 10 MD steps, the system is checked for potential bond formations. In this way, it typically takes 400 000 $\sim$ 500 000 MD steps to reach 90% conversion. Due to the periodic boundary condition in the lateral surfaces, the epoxy/Cu biamterial so constructed actually represents an infinite layer of epoxy attached to a Cu substrate. We note that the epoxy layer interacts with the Cu substrate via the Lennard-Jones potential given by equation (6).

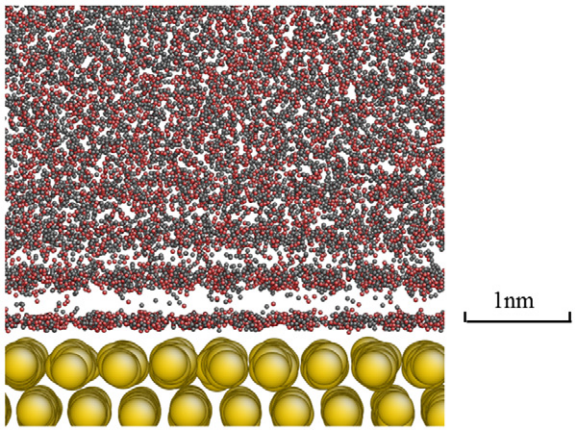

Figure 4. Zoomed-in view of the interfacial zone. Gray and red beads are the EPN and BPA beads, respectively. Yellow beads are the Cu beads.

3.3. Simulation of tensile deformation

The tensile deformation of the bimaterial is simulated by prescribing a downward rigid-body velocity to the Cu substrate while fixing the very top layer (∼1 nm thick) of the epoxy block. The prescribed downward velocity corresponds to a strain rate of $10^8\ s^{-1}$ in the epoxy block. The temperature is kept constant at 300 K using the Langevin thermostat [36] with the equation of motion being formulated as:

$$m\ddot{\boldsymbol{r}}_i = \boldsymbol{f}_i - m\Gamma\dot{\boldsymbol{r}}_i + \boldsymbol{W}_i(t), \tag{7}$$

where Γ is the damping constant and $\boldsymbol{W}_i$ is a random noise term. They satisfy the relation [37]

$$\left\langle \boldsymbol{W}_i(t)\boldsymbol{W}_j\left(t'\right)\right\rangle = 6k_{\mathrm{B}}Tm\Gamma\delta_{ij}\delta\left(t-t'\right), \tag{8}$$

where k_{B} is the Boltzmann, T is the absolute temperature, m is the mass of the beads, δ_{ij} is the Kronecker delta, and $\delta(t)$ is the Dirac delta function. The last two terms on the right-hand side of (7) couple the system to a heat bath which maintains a constant temperature. We found that using the Langevin thermostat is critical in keeping the system at a constant and uniform temperature.

4. Results and discussions

4.1. Epoxy microstructure near the interface

The microstructure of the epoxy molding compound near the substrate surface is of great interest. Geometric and energetic constraints may cause structural inhomogeneity in the epoxy near the interface. Upon full equilibration at room temperature, the near-interface microstructure of the epoxy is analyzed. Figure 4 shows a zoomed-in view of the interfacial zone. To clearly demonstrate the microstructural features, the epoxy and BPA beads are not drawn to scale. A clear feature is that the epoxy beads tend to be densely packed into a few distinctive bands. The further away from the interface the bands are, the less distinctive the band structure becomes. Such a structural feature is due to the rather planar geometry of the substrate surface, and the Lennard-Jones interactions between epoxy and substrate beads. *Ab initio* calculations [24] have shown that the benzene rings have a strong adsorption to metal

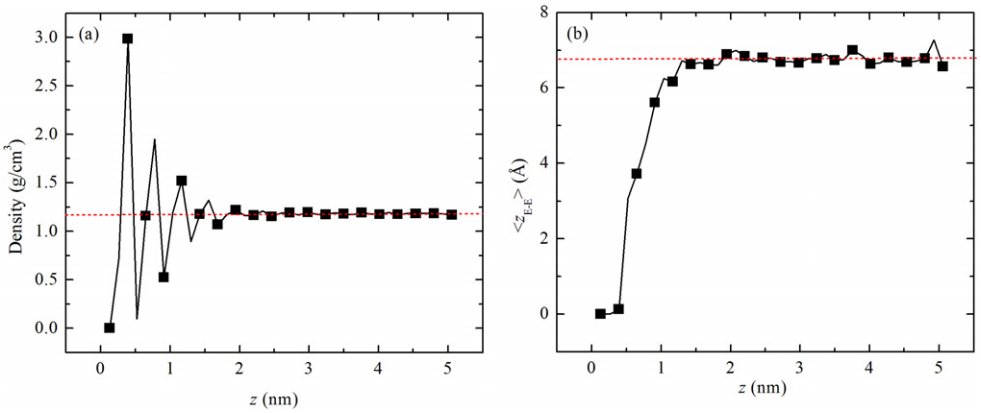

Figure 5. (*a*) Mass density versus z. (*b*) Projection onto the z-axis of the end-to-end distance of network strands $\langle z_{E-E}\rangle$ versus z-axis. The dashed lines represent the bulk values.

surfaces and prefer to align themselves in parallel with the Cu surface. In our previous full atomic studies of the same epoxy/Cu bimaterial [30], densely packed benzene rings were also observed near the interface. These existing *ab initio* and full atomic studies confirm that our CG model for the epoxy/Cu bimaterial is able to capture the structural characteristics of the epoxy/Cu interface at the atomistic level. More importantly, our CG model is able to capture the entire interfacial zone containing the heterogeneities.

To quantify the interfacial structural inhomogeneity observed in figure 4, and to determine how far it extends into the bulk epoxy, we studied the variation of some physical properties of the epoxy with respect to the z (normal direction) coordinate. In figure 5(*a*), we plot the mass density of the epoxy along the z-direction, where $z = 0$ is the interface, and $z = 80$ nm is at the top of the epoxy block. It clearly shows an oscillatory behavior within the range of about 2 nm from the interface, beyond which the mass density retains its bulk value, $\sim$1.18 g cm^{-3}. The oscillatory behavior of the density distribution agrees with the structural feature shown in figure 4, i.e. a few distinctive layers of densely packed epoxy beads near the interface. Another quantity of interest is the projection on the z-axis of the average end-to-end distance of polymer network strands, $\langle z_{E-E}\rangle$, which is plotted in figure 5(*b*) as function of the z coordinate. We note that $\langle z_{E-E}\rangle$ indicates how 'flat' a polymer strand is. If a strand is aligned parallel to the interface, then its two ends should be roughly on a plane parallel to the interface. Thus, its projection onto the z-axis, $\langle z_{E-E}\rangle$ should be almost zero. If a strand is not flat, $\langle z_{E-E}\rangle$ should be representative of the size of the strand. Figure 5(*b*) shows the $\langle z_{E-E}\rangle$ versus z curve. It is seen that the strands near the interface are almost flat, and the flatness rapidly disappears away from the interface. Beyond about 2 nm, the strands recover their bulk configuration. The results shown in figures 5(*a*) and (*b*) are consistent in that they indicate the same range of structural inhomogeneity near the interface.

4.2. Stress–strain curve and deformation behavior

By using the tensile simulation described in section 3, the stress–strain curve is obtained and shown in figure 6 for a strain rate of 10^8 s^{-1}. The stress–strain behavior shows an elastic response until the stress reaches a yield strength of $\sim$260 MPa at a strain of $\sim$5.4%. Beyond that, the bimaterial experiences a drastic relaxation of stress down to $\sim$125 MPa, which is due to

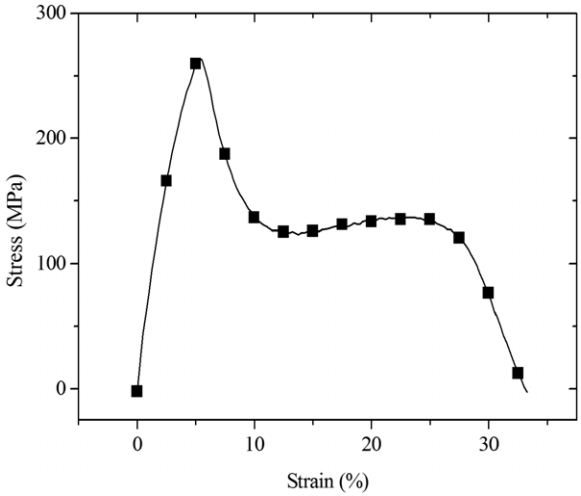

Figure 6. Stress–strain curves for the tensile simulation of epoxy/Cu bimaterial.

the nucleation of cavities [22]. Such cavitation is caused by the tri-axial stress state with a strong dilatational component. The tri-axial stress state is a consequence of the periodic boundary conditions prescribed in the lateral direction. In most practical applications, adhesives are indeed under such tri-axial state of stress due to constraints from the adherends. At about 25% strain, the stress decreases drastically, leading to the final interfacial failure.

In figure 7, several snapshots of the deformed configuration are shown. It is seen that at 15% strain, cavities start to nucleate in the epoxy near the interface because of the relatively weaker force-field between the epoxy and the Cu substrate. The cavitation is also accompanied by extension of the polymer network strands from their coiled states to taut conformations. Although not shown here, networks of polymer strands holding the inner wall of the cavities are observed inside the cavities [22].

After yielding and stress relaxation, a weak strain hardening takes place that extends to about 25% strain. This behavior is accompanied by expansion of the cavities. The second snapshot of figure 7 shows both longitudinally and laterally enlarged voids compared to the first snapshot. At the meantime, polymer strands are continuously transformed from their closed-packed to linear configurations. Upon reaching ultimate failure at a strain of 25%, the epoxy within the interfacial zone is fully stretched. The strong covalent bonds between the polymer beads prevent further deformation within the epoxy. Therefore, the polymer strands are pulled off from the Cu substrate as shown in the snapshot at 30% strain in figure 7. Such debonding eventually leads to a rather clean interfacial separation between the epoxy and the substrate as shown in the snapshot at 40% in figure 7.

To investigate the deformation, the displacement profile within the epoxy is plotted in figure 8(a) under three strain levels. The z-axis (horizontal) in figure 8(a) is the Lagrangian coordinate in that it indicates the location of the material particle in the undeformed state. For example, according to figure 8(a), the displacement at is about 4 nm under 5% of strain, while the displacement at $z = 80$ is zero. This means that the epoxy beads at the epoxy/Cu interface ($z = 0$) before the deformation have been displaced by 4 nm (downward) when the overall strain of the bimaterial is at 5%, while the epoxy beads originally located at the top of the epoxy block ($z = 80$ nm) remain fixed when the overall strain is 5%.

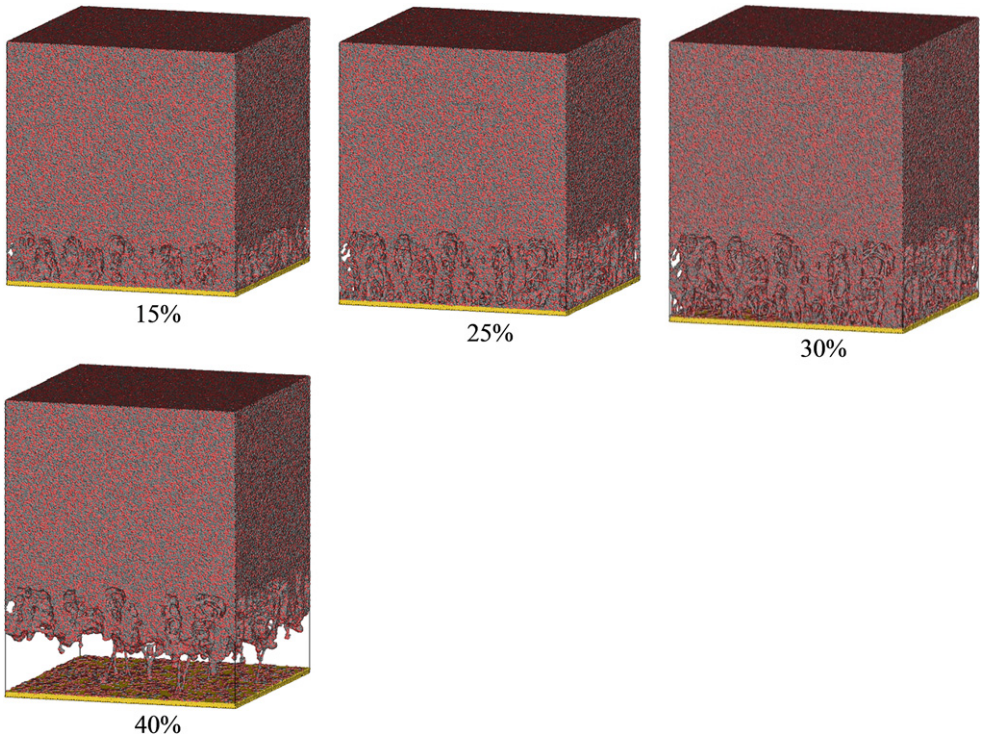

Figure 7. Snapshots of the deformation process for the 90% cross-linked epoxy/Cu bimaterial under tension at a strain rate of 10^8 s^{-1}.

Several interesting observations can be made from figure 8(*a*). First, the displacement profile before yielding (strain $\leqslant$5%) is nearly linear, which means that the strain (slope of the displacement profile) of the epoxy is nearly a constant. Second, after yielding, the deformation in the epoxy is highly localized to a thin ($\sim$10 nm) zone next to the interface. Calculated from the slope of curves in figure 8(*a*), the average strain inside the interfacial zone is approximately 115% when the overall strain is 15%, and approximately 185% when the overall strain is 25%. Outside this interfacial zone, the strain in the epoxy remains at about 2% everywhere at both 15% and 25% strain levels. In fact, although not shown, once yielding occurs, the strain outside the interfacial zone remains at $\sim$2%, irrespective of the overall strain level. This suggests that the increased overall strain after yielding is all caused by deformation of epoxy within the interfacial zone. Finally, upon yielding, the average strain outside the epoxy drops from $\sim$5% to $\sim$2%. This is caused by the cavitation-induced softening of the epoxy inside the interfacial zone, which causes yielding and stress relaxation of the epoxy inside the interfacial zone.

The localization of deformation has been uncovered by MD/continuum simulations [38] and experiments [39] for nano-particle reinforced polymer composites. In [39], strain concentration reaches over 200% between nano-particle fillers while the overall strain is only 15%. Regarding the thickness of the interfacial zone, in [40], the thickness of the interphase between a polymer and a nano-particle is estimated to be 6–7 nm from the measurement of polymer chain dynamics, which is similar to our value.

We note that in our previous full atomic studies [6] on the same epoxy/Cu bimaterial, such highly localized deformation was not observed. The reason for this is that the material volume

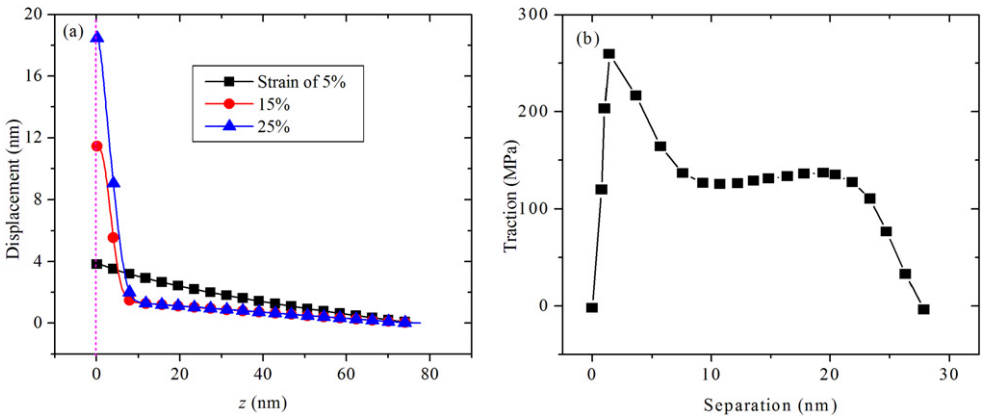

Figure 8. (*a*) Displacement as a function of distance to the substrate along the normal direction for the 90% cross-linked epoxy/Cu bimaterial under three overall strain levels. (*b*) The extracted traction–separation relationship based on the definition of the interfacial zone.

used in the full atomic investigation is less than the size of the interfacial zone, and thus unable to capture the localized deformation. This demonstrates the necessity of accessing the correct length scale to fully understand the mechanical behavior of polymeric materials.

Further, figure 8(*a*) also indicates that the thickness of the interfacial zone increases with increasing applied load. In figure 8(*a*), the displacement for the epoxy beads at the top of the interfacial zone ($z = 10$ nm) remains the same for the overall strain of 15% and 25%, implying that their positions stay roughly unchanged. On the other hand, epoxy beads in the vicinity of the substrate ($z = 0$ nm) show additional displacement. Therefore, the thickness of the interfacial zone increases. This apparent increase of the interfacial zone thickness is entirely due to the increased deformation inside the interfacial zone. The total mass of the interfacial zone remains unchanged. This discovery motivates the use of a cohesive zone model in the macroscopic scale where the epoxy/Cu bimaterial is treated as a continuum. Thus, as the applied load increases, the initial thickness of the interfacial zone is stretched or elongated. Such elongation of the interfacial zone thickness can be defined as the separation between the Cu surface and the bulk epoxy at the continuum scale. The relationship between this interfacial separation and the applied tensile stress can be easily obtained by keeping track of the displacement profile at each load increment. For example, it follows from figure 8(*a*) that the separation is about 1.5 nm and 8.5 nm, respectively, when the applied overall strain is 15% and 25%. From figure 6, we find that the applied tensile stresses are 125 MPa and 130 MPa at 10% and 25% strain, respectively. Thus, one may conclude when the separation is 1.5 nm, the corresponding stress is 125 MPa, and when the separation is 8.5 nm, the corresponding stress is 130 MPa. Since the applied tensile stress is the same as the traction at the interface, the applied tensile stress versus separation relationship gives the desired traction versus separation law used in the cohesive zone model in continuum mechanics. The results are plotted in figure 8(*b*). It is seen that the traction versus separation curve in figure 8(*b*) shows the general features of traction versus separation laws for polymer/metal interfaces. The traction first increases almost linearly with increasing separation. Once reaching its maximum, the traction drops drastically, followed by a weak strain hardening until reaching the cohesive strength and critical separation.

We comment that the cohesive zone model is one of the most commonly used constitutive laws to describe the deformation and failure of material interfaces [41, 42]. However, in most

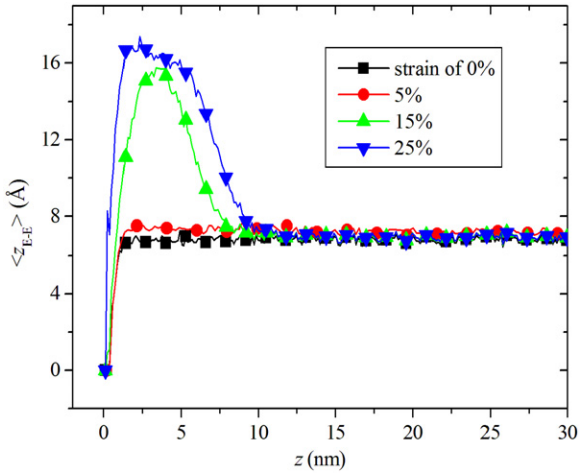

Figure 9. End–end distance (projection to the normal axis) of network strands along the normal direction at different overall strain levels.

applications, the traction versus separation relationship is assumed *ad hoc* and calibrated via indirect experimental observations. Figure 8(*b*) is the first traction versus separation relationship for polymer/metal interfaces predicted based on the atomic microstructure at the interface.

During tensile deformation, the configuration of epoxy network strands also evolves. As shown in figure 5(*b*), in the undeformed state, $\langle z_{E-E} \rangle$ has a uniform value of 6.7 Å except for strands very close (<2 nm) to the Cu substrate. Upon tensile deformation, it is expected that $\langle z_{E-E} \rangle$ for the near-surface strands should increase, since, according to figure 7, strands near the interface are being pulled to align with the loading direction. This is confirmed by the results shown in figure 9, which plots the $\langle z_{E-E} \rangle$ versus z curves under different overall strains. Before yielding, for example, at 5% overall strain, the $\langle z_{E-E} \rangle$ versus z curve is almost the same as that at 0% overall strain (undeformed configuration). After yielding, for example, at 15% strain, the $\langle z_{E-E} \rangle$ versus z curve profile shows a peak within the interfacial zone $0 < z < 10$ nm, and the height of the peak increases with increasing overall strain. This confirms our earlier expectations that the network strands within the interfacial zone are being pull to align with the direction of the applied load.

Although polymer strands are being continuously re-orientated toward the loading direction during the deformation, very few of them are broken. Even within the interfacial zone where the strain is highly localized, the number of broken bonds is less than 0.05% during the entire deformation process. At failure, the polymer strands are simply peeled off from the Cu substrate. In other words, the failure is dominantly adhesive at the epoxy/Cu interface rather than cohesive within the epoxy.

4.3. Effects of strain rate and temperature

The epoxy/Cu bimaterial's mechanical behavior can be affected by strain rate and temperature. Due to the large number of beads (~8 million) in our simulation model, the quasistatic loading rates used in typical laboratory tests are beyond our reach. Nevertheless, to investigate the dependence on the loading rates, we simulated the tensile deformation with two loading rates, $10^8\ s^{-1}$ and $2 \times 10^7\ s^{-1}$, at room temperature (300 K). The resulting stress–strain curves are

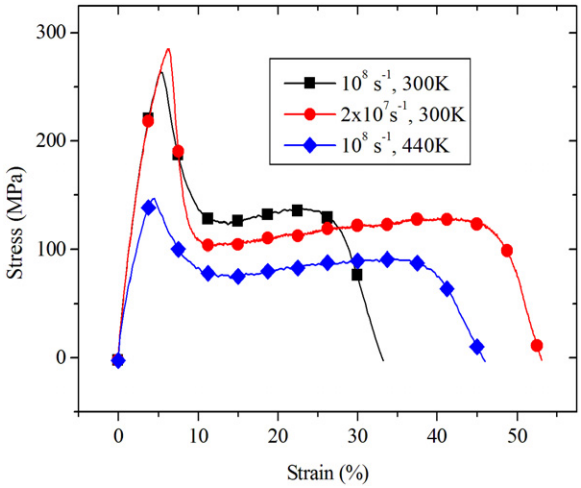

Figure 10. Stress–strain curves for lower strain rate and higher temperature.

plotted in figure 10. The red circles are for the loading rate of 2×10^7 s^{-1} and the black squares are for 10^8 s^{-1}. It is seen that the strain rate (within the range considered) affects only the post-yielding behavior. As expected, deformation at lower loading rates is more ductile in that the stress–strain curve at this lower rate has a longer post-yielding strain hardening regime with a lower stress magnitude, leading to a larger failure strain.

In addition to the more ductile behavior, the interfacial zone is thicker at lower loading rates. This can be seen from the snapshots in figure 11 and the displacement profiles shown in figure 12(*a*). The thicker interfacial zone is consistent with the more ductile behavior because most of the inelastic deformation occurs within the interfacial zone; thus, the thicker interfacial zone leads to a large deformation. In fact, it can be easily seen that the strain outside the interfacial zone is the same under both loading rates. The increased ductility comes from the increased interfacial zone where strain is highly localized.

Based on the displacement profiles in figure 12(*a*) and the stress–strain curves in figure 10, the corresponding traction versus separation relationship can be obtained for the different loading rates considered. The results are shown in figure 12(*b*). As expected, the interface is more ductile at lower loading rates in that the cohesive strength is lower and the separation from failure is larger.

From the second and third snapshots in figure 11 one can observe that the post-yielding behavior at the lower loading rate is also caused by cavity growth and polymer chain stretching/breaking. The ultimate failure is caused by polymer strands peeling off the Cu substrate. However, since the interfacial zone is thicker at lower loading rates, cavities are larger, and the probability of bond breaking is thus higher since more polymer strands experience re-orientation along the loading axis. The latter is demonstrated in figure 13, which plots the number density of broken bonds within the interfacial zone.

To investigate the effect of temperature, simulations were conducted for tensile tests at 440 K. Previous studies [6, 7, 22] have shown that the epoxy considered here has a T_g of ∼400 K. Therefore, at 440 K, the epoxy is in its rubbery state. Before the tensile simulation starts, it is necessary to re-conduct the cooling process from the curing temperature (500 K) to 440 K and the subsequent equilibration at this temperature. The stress–strain curve of the uniaxial strain deformation is presented in figure 10 by the curve with the blue diamond symbols. It is

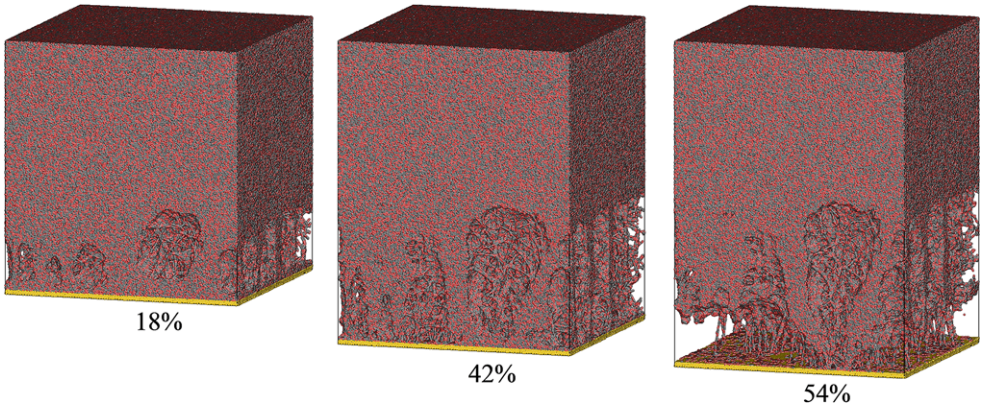

Figure 11. Snapshots of the configurations of the 90% cross-linked epoxy/Cu bimaterial during the tensile deformation using the strain rate of $2 \times 10^7\ s^{-1}$.

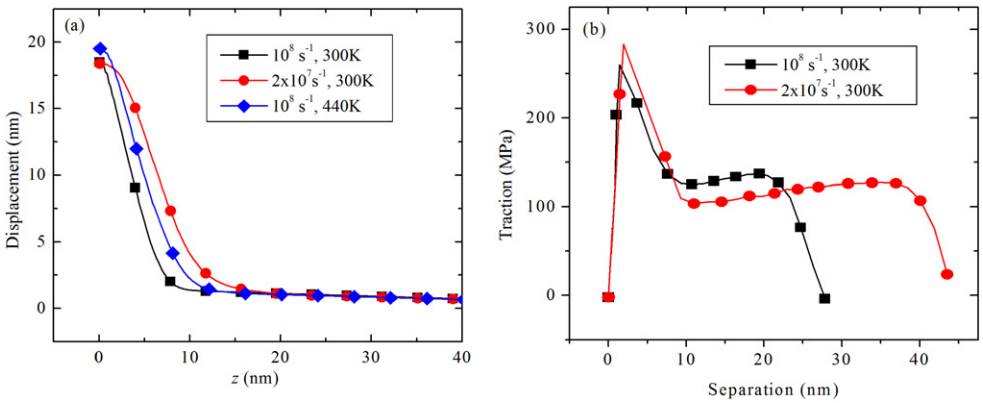

Figure 12. (*a*) Displacement as a function of distance to the substrate for lower strain rate and higher temperature. (*b*) Traction–separation relationship for the lower strain rate.

seen that the high temperature significantly lowers the yielding strength to ∼145 MPa. Since the epoxy is in its rubbery state, the lowered yield strength is obviously a reflection of the temperature dependency of the epoxy's yielding strength. Beyond yielding, the epoxy/Cu bimaterial experiences similar strain hardening until reaching failure at a strain of ∼36%.

Another observation is that the effect of higher temperature on the uniaxial strain behavior is similar to that of lower loading rates. For example, figure 12(*a*) indicates that higher temperatures result in a thicker interfacial zone, similar to the case of a lower loading rate. Also, figure 13 shows that more bonds are broken within the interfacial zone at higher temperatures, just like the case with a lower loading rate.

4.4. Effect of conversion

Conventionally, conversion measures the cross-link density in a polymer. In our CG model, a cross-link is a bead that has at least three strands reaching out to other such beads. Since all the beads have the same mass, a conversion of 90% in our CG model means that 90% of the reactive beads are reacted. Up to this point, all the examples discussed in this paper are

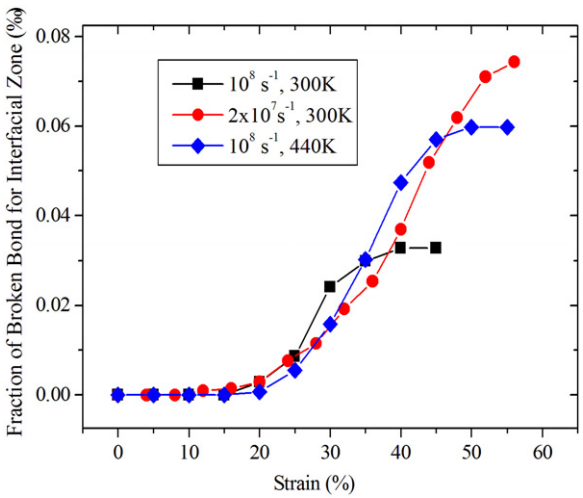

Figure 13. Fraction of broken bonds within the interfacial zone versus strain for different strain rates and temperatures.

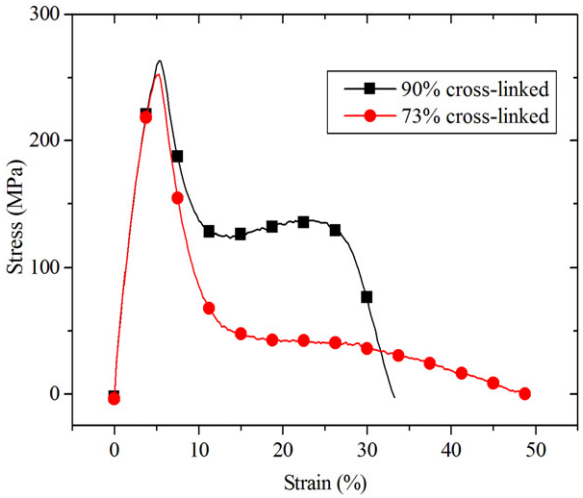

Figure 14. Stress–strain curve for an epoxy/Cu bimaterial with 73% epoxy conversion.

for epoxy with 90% conversion. It is of interest to investigate the case of lower conversion. To this end, an example of 73% conversion was considered. The corresponding stress–strain curve is plotted in figure 14. It is seen that after yielding there is no strain hardening regime in the stress–strain behavior of the epoxy/Cu bimaterial with lower conversion. Instead, the stress drastically drops to ∼43 MPa, then maintains at a plateau for a short range of strain, and finally, gradually decays to zero. Figure 15 shows the atomic configurations during the tensile deformation. The first snapshot (with strain of 20%) indicates the formation of fibril-like microstructures that resemble 'crazing' in thermoplastics: vertical ligaments are observed that bridge the bulk epoxy to a thin layer of epoxy on the substrate surface. This is due to the fact that epoxy with lower conversion tends to have a less cross-linked network structure. This

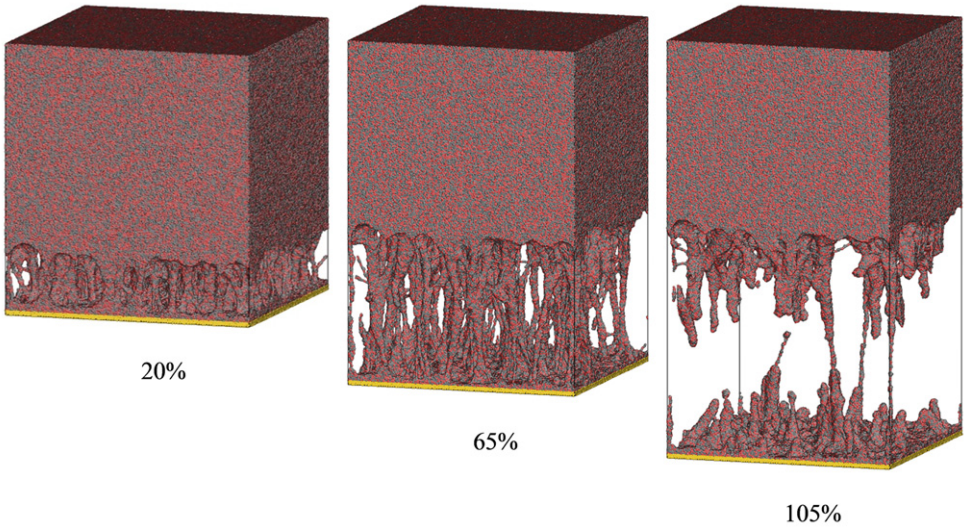

Figure 15. Snapshots of the configurations of the 73% cross-linked epoxy/Cu bimaterial during the tensile deformation.

can be demonstrated by the difference in the number density of elastically effective chains, defined as the network strands between two cross-links. The number density of elastically effective chains is roughly $1.4 \times 10^{21}\,\mathrm{cm}^{-3}$ at 90% conversion, and $7.9 \times 10^{20}\,\mathrm{cm}^{-3}$ at 73% conversion. The much lowered cross-link density makes it easier to form ligaments that lack links among them, i.e., the crazing-like microstructure shown in the first snapshot of figure 15. The much lowered stress magnitude in the post-yielding regime of the stress–strain curve can be explained by the larger volume fraction of cavities in the lower conversion epoxy, which is again related to the lower density of elastically effective chains. Further deformation involves the thickening of the crazing bands. This process is seen in the second snapshot in figure 15, in which the ligaments are significantly stretched as compared to the first snapshot. Stretching of the ligaments can be confirmed by studying the number fraction of broken bonds within the interfacial zone, which is shown in figure 16. It is seen that from the strain of 20% to 80%, there is a sharp increase in the number of broken bonds in the case of 75% conversion. When the strain reaches about 80%, most of the ligaments are broken which leads to the final failure. This corresponds to the configuration shown in the third snapshot in figure 15. In the failed bimaterial, the Cu substrate is fully covered by a thin layer of epoxy. In other words, the failure mode with 73% conversion is cohesive rather than adhesive (interfacial).

As can be observed in figure 15, the plastic deformation mechanisms, specifically, the formation of the band of ligaments and the subsequent stretching/scission of the ligaments, is localized in the interfacial zone. Following the discussion in section 4.2, the displacement profile was obtained for the epoxy/Cu bimaterial with 73% conversion, from which the interfacial zone is found to be ∼10 nm. Combining the displacement profile with the stress–strain curve shown in figure 14 yields the corresponding traction–separation relationship shown in figure 17. The cohesive strength is ∼65 MPa at the separation of ∼21 nm. However, due to the ductile behavior of the interfacial zone, the traction decays gradually after reaching the strength and does not vanish until ∼54 nm. Therefore, the critical separation at which the interfacial zone completely fails is 54 nm.

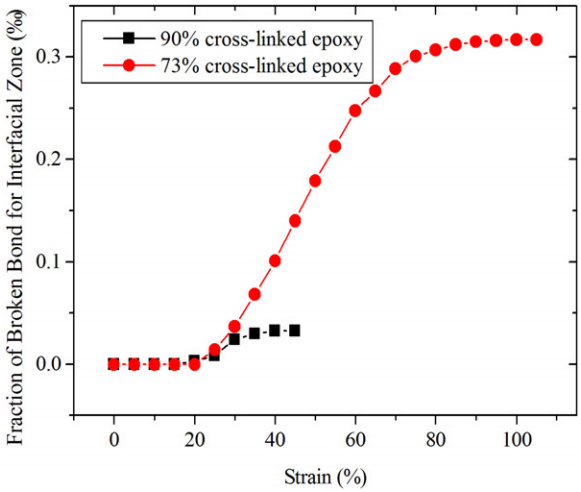

Figure 16. Fraction of broken bonds as a function of strain within the interfacial zone versus strain for different conversions.

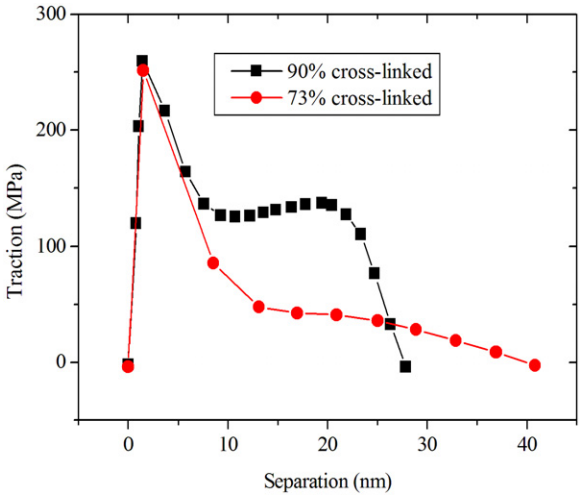

Figure 17. Traction–separation relationship for different conversions.

5. Summary and conclusion

In this article, a coarse-grained study of the interface between a cross-linked epoxy and a Cu substrate is presented. The bulk epoxy is modeled by a CG model developed in our earlier studies [22, 23]. To parametrize the CG potential describing the interfacial interactions at the epoxy/Cu interface, the interfacial free energy landscape is first computed by the full atomic MD simulations in conjunction with a metadynamics method. The same is then computed using the CGMD, in which the interfacial potential parameters are optimized until the interfacial free energy landscape matches that calculated from the full atomic MD.

The newly developed CG model is then used to simulate the uniaxial strain deformation of an epoxy/Cu bimaterial. The simulation model is $\sim 89 \times 89 \times 79\,\text{nm}^3$ and consists of nearly 8 million beads. Based on the simulation results, the following conclusions can be drawn.

First, for highly cross-linked epoxy (90% conversion), the initial deformation of the epoxy/Cu bimaterial is almost linearly elastic. Plastic deformation occurs via cavity nucleation and growth as well as polymer chain stretching and breaking in the epoxy. After yielding, the plastic strain is highly localized in a thin layer of epoxy next to the epoxy/Cu interface. Further increase of the deformation only increases the plastic deformation within this layer of epoxy, called the interfacial zone, while the strain in the bulk epoxy remains unchanged with the increasing overall deformation. Consequently, the thickness of the deformed interfacial zone increases with increasing overall deformation. By relating the traction to the change in the thickness of the deformed interfacial zone, a traction–separation relationship can be established from the CGMD simulations. This traction–separation relationship can then be used in the cohesive zone model in a continuum mechanics modeling of the epoxy/Cu interface.

Second, as expected, the mechanical behavior of the epoxy/Cu depends on the loading rate and the temperature. A lower loading rate or higher temperature makes the bimaterial more ductile and vice versa. A lower loading rate or higher temperature also increases the initial thickness of the interfacial zone. For example, the initial interfacial zone is 10 nm and 20 nm at the strain rates of $10^8\ s^{-1}$ and $5 \times 10^7\ s^{-1}$, respectively.

Finally, a lower conversion rate or lower cross-link density in the epoxy tends to change the failure mode from adhesive (interfacial) to cohesive. At 73% conversion, for example, failure is dominantly cohesive in that the failure occurs within the epoxy near the epoxy/Cu interface, leaving a thin layer of epoxy residual on the Cu surface.

To close, we mention that, as in most molecular level simulations, the strain rates used in this study are orders of magnitude higher than the quasistatic strain rate used in typical laboratory tests. Thus, whether the simulations can provide quantitative predictions of material behavior under laboratory test conditions remains an open question.

Acknowledgment

The work was supported in part by a grant from NSF (CMMI-1200075).

References

[1] Yu J, Song J Y and Park I S 2002 Analyses of the practical adhesion strengths of the metal/polymer interfaces in electronic packaging *J. Electron. Mater.* **31** 1347–52
[2] Cho K W and Cho E C 2000 Effect of the microstructure of copper oxide on the adhesion behavior of epoxy/copper leadframe joints *J. Adhes. Sci. Technol.* **14** 1333–53
[3] Creton C *et al* 2002 Adhesion and fracture of interfaces between immiscible polymers: from the molecular to the continuum scale *Mol. Simul. Fract. Gel Theory* **156** 53–136
[4] Lau D, Buyukozturk O and Buehler M J 2012 Characterization of the intrinsic strength between epoxy and silica using a multiscale approach *J. Mater. Res.* **27** 1787–96
[5] Wong C K Y *et al* 2012 Establishment of the coarse grained parameters for epoxy–copper interfacial separation *J. Appl. Phys.* **111** 094906
[6] Yang S, Gao F and Qu J 2013 A molecular dynamics study of tensile strength between a highly-crosslinked epoxy molding compound and a copper substrate *Polymer* **54** 5064–74
[7] Yang S and Qu J 2012 Computing thermomechanical properties of crosslinked epoxy by molecular dynamic simulations *Polymer* **53** 4806–17
[8] Sun H 1995 *Ab-initio* calculations and force-field development for computer-simulation of polysilanes *Macromolecules* **28** 701–12
[9] Sun H 1994 Force-field for computation of conformational energies, structures, and vibrational frequencies of aromatic polyesters *J. Comput. Chem.* **15** 752–68
[10] Li Y *et al* 2013 Challenges in multiscale modeling of polymer dynamics *Polymers* **5** 751–832

[11] Padding J T and Briels W J 2011 Systematic coarse-graining of the dynamics of entangled polymer melts: the road from chemistry to rheology *J. Phys.: Condens. Matter* **23** 233101
[12] Kremer K and Muller-Plathe F 2002 Multiscale simulation in polymer science *Molecular Simulation* **28** 729–50
[13] Fukunaga H, Takimoto J and Doi M 2002 A coarse-graining procedure for flexible polymer chains with bonded and nonbonded interactions *J. Chem. Phys.* **116** 8183–90
[14] Vettorel T and Meyer H 2006 Coarse graining of short polythylene chains for studying polymer crystallization *J. Chem. Theory Comput.* **2** 616–29
[15] Shelley J C *et al* 2001 A coarse grain model for phospholipid simulations *J. Phys. Chem.* B **105** 4464–70
[16] Li Y *et al* 2012 A predictive multiscale computational framework for viscoelastic properties of linear polymers *Polymer* **53** 5935–52
[17] Murtola T *et al* 2004 Coarse-grained model for phospholipid/cholesterol bilayer *J. Chem. Phys.* **121** 9156–65
[18] Izvekov S and Voth G A 2005 A multiscale coarse-graining method for biomolecular systems *J. Phys. Chem.* B **109** 2469–73
[19] Marrink S J, de Vries A H and Mark A E 2004 Coarse grained model for semiquantitative lipid simulations *J. Phys. Chem.* B **108** 750–60
[20] Marrink S J *et al* 2007 The MARTINI force field: coarse grained model for biomolecular simulations *J. Phys. Chem.* B **111** 7812–24
[21] Shinoda W, Devane R and Klein M L 2007 Multi-property fitting and parameterization of a coarse grained model for aqueous surfactants *Mol. Simul.* **33** 27–36
[22] Yang S, Cui Z and Qu J 2014 A coarse-grained model for epoxy molding compound *J. Phys. Chem.* B **118** 1660–9
[23] Yang S and Qu J 2014 Coarse-grained molecular dynamic simulations of the tensile behavior of a thermosetting polymer *Phys. Rev.* E **90** 012601
[24] Delle Site L *et al* 2002 Polymers near metal surfaces: selective adsorption and global conformations *Phys. Rev. Lett.* **89** 156103
[25] Abrams C F., Delle Site L and Kremer K 2003 Dual-resolution coarse-grained simulation of the bisphenol-A-polycarbonate/nickel interface *Phys. Rev.* E **67** 021807
[26] Farah K *et al* 2011 Interphase formation during curing: reactive coarse grained molecular dynamics simulations *J. Phys. Chem.* C **115** 16451–60
[27] Iwamoto N 2012 Developing the stress–strain curve to failure using mesoscale models parameterized from molecular models *Microelectron. Reliab.* **52** 1291–9
[28] Iwamoto N 2012 Molecularly derived mesoscale modeling of an epoxy/Cu interface (part III*): Interface roughness *13th Int. Conf. on Thermal, Mechanical and Multi-Physics Simulation and Experiments in Microelectronics and Microsystems (EuroSimE)*, Libson, Portugal
[29] Iwamoto N 2010 Mechanical properties of an epoxy modeled using particle dynamics, as parameterized through molecular modeling *11th Int. Conf. on Thermal, Mechanical & Multi-Physics Simulation, and Experiments in Microelectronics and Microsystems (EuroSimE)*, Bordeaux, France
[30] Yang S, Gao F and Qu J 2013 A molecular dynamics study of tensile strength between a highly-crosslinked epoxy molding compound and a copper substrate *Polymer* **54** 5064–74
[31] Stevens M J 2001 Interfacial fracture between highly cross-linked polymer networks and a solid surface: effect of interfacial bond density *Macromolecules* **34** 2710–18
[32] Laio A and Gervasio F L 2008 Metadynamics: a method to simulate rare events and reconstruct the free energy in biophysics, chemistry and material science *Rep. Prog. Phys.* **71** 126601
[33] Laio A and Parrinello M 2002 Escaping free-energy minima *Proc. Natl Acad. Sci. USA* **99** 12562–6
[34] Plimpton S 1995 Fast parallel algorithms for short-range molecular-dynamics *J. Comput. Phys.* **117** 1–19
[35] Bonomi M *et al* 2009 PLUMED: A portable plugin for free-energy calculations with molecular dynamics *Comput. Phys. Commun.* **180** 1961–72

[36] Schneider T and Stoll E 1978 Molecular-dynamics study of a three-dimensional one-component model for distortive phase transitions *Phys. Rev.* B **17** 1302–22
[37] Kubo R 1966 The fluctuation–dissipation theorem *Rep. Prog. Phys.* **29** 255–84
[38] Greene M S *et al* 2014 The archetype-genome exemplar in molecular dynamics and continuum mechanics *Comput. Mech.* **53** 687–737
[39] Akutagawa K *et al* 2008 Mesoscopic mechanical analysis of filled elastomer with 3D-finite element analysis and transmission electron microtomography *Rubber Chem. Technol.* **81** 182–9
[40] Li Y, Kroger M and Liu W K 2014 Dynamic structure of unentangled polymer chains in the vicinity of non-attractive nanoparticles *Soft Matter* **10** 1723–37
[41] Needleman A 1987 A continuum model for void nucleation by inclusion debonding *J. Appl. Mech.-Trans. ASME* **54** 525–31
[42] Tvergaard V and Hutchinson J W 1996 On the toughness of ductile adhesive joints *J. Mech. Phys. Solids* **44** 789–800